

---

# Automatic Differentiation is Essential in Training Neural Networks for Solving Differential Equations

---

**Chuqi Chen\***

Department of Mathematics  
Hong Kong University of Science and Technology  
Clear Water Bay, Hong Kong SAR, China  
cchenck@connect.ust.hk

**Yahong Yang\***

Department of Mathematics  
The Pennsylvania State University, University Park,  
State College, PA, USA  
yxy5498@psu.edu

**Yang Xiang†**

Department of Mathematics  
Hong Kong University of Science and Technology  
Clear Water Bay, Hong Kong SAR, China  
and  
Algorithms of Machine Learning and Autonomous Driving Research Lab  
HKUST Shenzhen-Hong Kong Collaborative Innovation Research Institute  
Futian, Shenzhen, China  
maxiang@ust.hk

**Wenrui Hao†**

Department of Mathematics  
The Pennsylvania State University, University Park,  
State College, PA, USA  
wxh64@psu.edu

## Abstract

Neural network-based approaches have recently shown significant promise in solving partial differential equations (PDEs) in science and engineering, especially in scenarios featuring complex domains or the incorporation of empirical data. One advantage of neural network method for PDEs lies in its automatic differentiation (AD), which necessitates only the sample points themselves, unlike traditional finite difference (FD) approximations that require nearby local points to compute derivatives. In this paper, we quantitatively demonstrate the advantage of AD in training neural networks. The concept of truncated entropy is introduced to characterize the training property. Specifically, through comprehensive experimental and theoretical analyses conducted on random feature models and two-layer neural networks, we discover that the defined truncated entropy serves as a reliable metric for quantifying the residual loss of random feature models and the training speed

---

\*Equal contributions

†Corresponding Authors

of neural networks for both AD and FD methods. Our experimental and theoretical analyses demonstrate that, from a training perspective, AD outperforms FD in solving partial differential equations.

## 1 Introduction

Neural networks have been extensively applied in solving partial differential equations (PDEs) [24, 31, 9, 27, 12, 8, 3, 4, 14], particularly in addressing high-dimensional problems, complex domains, and incorporating empirical data. Approaches like Physics-Informed Neural Networks (PINNs) [24, 21, 29] and the deep Ritz method [31, 17] have demonstrated this approach. In solving PDEs, the computation of derivatives within the loss functions is crucial. This can be implemented through two main methods: automatic differentiation (AD), leveraging the recursive nature of neural networks [2, 24, 5], and numerical differentiation, such as finite difference (FD) methods [7, 19, 15, 20]. However, there is a significant discrepancy in the training performance between these two differentiation approaches (see Fig. 1 right), with AD outperforming FD. Motivated by this difference, this paper specifically delves into analyzing the training error of these two methods.

In this paper, we compare AD and FD methods for PDEs by training two-layer neural networks and the random feature model (RFM) [4]. Both models follow the same structure as depicted in Eq. 3. The two-layer neural networks (NN) involve training all parameters, whereas the RFM fixes the inner layer parameters randomly and trains only the outer layer parameters. Specifically, the RFM addresses a convex optimization (least squares problem), solving  $\mathbf{A}\mathbf{a} = \mathbf{f}$ , where  $\mathbf{a}$  represents the outer layer parameters, as shown in Eq. 3. We refer to  $\mathbf{A}$  as the system matrix. In contrast, training the two-layer neural networks involves nonconvex optimization, tackled via gradient descent. The loss dynamics are expressed as  $\frac{\partial L}{\partial t} = -\mathbf{e}^\top \mathbf{G}\mathbf{e}$ , where  $L = \mathbf{e}^2$  denotes the loss function in PDE solving, and  $\mathbf{G}$  represents the kernel of the gradient descent.

Our analysis is grounded in eigenvalue studies in training process, shedding light on the distinct behaviors exhibited by AD and FD in PINN frameworks. We observe that different differentiation methods influence both  $\mathbf{A}$  and  $\mathbf{G}$ , thereby affecting the training process. By analyzing the singular values or eigenvalues of  $\mathbf{A}$  and  $\mathbf{G}$  derived from these differentiation methods, we find that training performance is closely tied to these values. Our theoretical and experimental analyses indicate that AD outperforms FD methods. In RFM, AD achieves a smaller residual error (i.e., training error), as illustrated in Fig. 1(b). In two-layer neural networks, AD facilitates faster gradient descent dynamics compared to FD, leading to a more rapid decrease in the loss function.

Based on theoretical analysis and computational experiments, we observe that the singular values of matrices  $\mathbf{A}$  and  $\mathbf{G}$  exhibit similar characteristics in both the AD and FD methods. Notably, the large singular values are nearly identical due to the relatively small numerical differentiation errors introduced by FD (Proposition. 1). However, we observe that the small singular values of FD are larger than those of AD, primarily due to the impact of numerical differentiation errors on these smaller values (Proposition. 2). Therefore, in the RFM, a truncated singular value approach is necessary to solve  $\mathbf{A}\mathbf{a} = \mathbf{f}$  by computing a pseudoinverse of  $\mathbf{a}$ , where only singular values greater than the truncated value are inverted. Since FD retains more small singular values than AD, this discrepancy leads to higher training errors for FD. These small singular values, while contributing less to approximation error, significantly impact training error, explaining AD's better performance in the RFM. Similarly, in two-layer neural networks, the abundance of small values in  $\mathbf{G}$  for FD slows down the training process in gradient descent methods, resulting in slower training compared to AD.

To quantify this observation, we introduce the following two definitions to measure the number of small singular values near the truncation threshold:

**Definition 1 (Effective cut-off number).** Let  $\mathbb{S}$  represent the set of singular values of matrix  $\mathbf{A}$  and  $\sigma_{\max}$  is the largest singular value of  $\mathbf{A}$ . We define a function  $e_{\mathbf{A}}(a)$  that denotes the count of singular values in set  $\mathbb{S}$  that do not exceed a given value, denoted by  $a \cdot \sigma_{\max}$  ( $0 \leq a < 1$ ). Mathematically, this can be expressed as:

$$e_{\mathbf{A}}(a) = |\{\sigma \in \mathbb{S} : \sigma \geq a \cdot \sigma_{\max}\}|, \quad (1)$$

where  $|\cdot|$  denotes the cardinality of this set.

Based on the effective cut-off number, we introduce the truncated entropy:

**Definition 2 (Truncated entropy).** For a matrix  $\mathbf{A} \in \mathbb{R}^{m \times n}$  with singular values  $\sigma_1 \geq \sigma_2 \geq \dots \geq \sigma_m$ , and a given  $a \geq 0$ , the truncation entropy of  $\mathbf{A}$  is defined as:

$$H_{\mathbf{A}}(a) = -\frac{1}{e_{\mathbf{A}}(a)} \sum_{k=1}^{e_{\mathbf{A}}(a)} p_k \log p_k, \quad (2)$$

where  $p_k = \frac{\sigma_k}{\|\boldsymbol{\sigma}\|_1}$  for  $k = 1, 2, \dots, e_{\mathbf{A}}(a)$ , with  $\boldsymbol{\sigma} = [\sigma_1, \sigma_2, \dots, \sigma_{e_{\mathbf{A}}(a)}]^T$ .

Note that the defined truncated entropy, which is a normalized version of the spectral entropy [25, 6] after truncation, plays a crucial role in our study. It reflects the impact of small singular values after truncation. Theoretical analysis, presented in Theorem 1 and Remark 1, demonstrates the effectiveness of the defined truncated entropy in quantifying the training speed of gradient descent. Specifically, the larger the value of  $H_{\mathbf{A}}(a)$ , the faster the training speed. Empirically, we observe a strong correlation between truncated entropy and training error, as depicted in Fig. 1. As the number of neurons increases, truncated entropy decreases, leading to an increase in training error. The truncated entropy of AD surpasses that of FD, indicating that AD achieves a lower training error compared to FD.

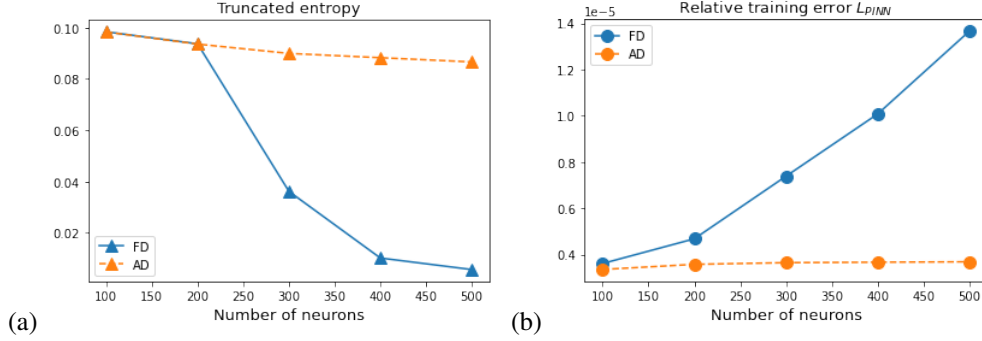


Figure 1: **(a):** Truncated entropy and **(b):** Relative training error  $L_{PINN}$  ( $\|\mathbf{A}\mathbf{a} - \mathbf{f}\|/\|\mathbf{f}\|$ ) are depicted for both AD and FD methods with varying numbers of neurons in RFM for solving  $u_{xx} = f(x)$  with Dirichlet boundary conditions. The exact solution is given by  $u(x) = \sin(\pi x)$ , where  $x \in [-1, 1]$ . (The number of sample points equals the number of neurons, and the effective cutoff number is  $e_{\mathbf{A}}(10^{-12})$ ).

We delve into a comparative analysis of the performance of automatic differentiation (AD) and finite difference (FD) methods within Physics-Informed Neural Networks (PINN) in Section 3. We present experimental results conducted in higher-dimensional spaces and for higher-order derivative PDEs, to validate our findings and demonstrate the consistency of results across varying dimensions and complexities in Section 4.

## 2 Neural Network Structure and Setups for Solving PDEs

In this section, we review two types of neural network models: two-layer neural networks and random feature models for solving the Poisson equation based on the Physics-Informed Neural Networks (PINNs) method [24]. We will extend our results to other equations in the computational experiments section.

### 2.1 Neural Network Structure

We focus on the two-layer neural network structure operating in a  $d$ -dimensional space, where there is only one hidden layer. The model is represented as:

$$\phi(\mathbf{x}; \boldsymbol{\theta}) = \sum_{j=1}^M a_j \sigma(\mathbf{w}_j \cdot \mathbf{x} + b_j), \quad \mathbf{x} \in \Omega \quad (3)$$

In this neural network,  $\boldsymbol{\theta}$  denotes all the parameters  $\{(a_j, \mathbf{w}_j, b_j)\}_{j=1}^M \subset \mathbb{R} \times \mathbb{R}^d \times \mathbb{R}$ , all of which are free parameters that need to be learned. Here,  $\sigma$  represents the nonlinear activation function. Due

to the inherent nonlinearity in this formulation, the learning process becomes nonconvex, posing challenges in optimization.

The random feature model is identical to Eq. 3, except that the inner parameters  $\{\mathbf{w}_j, b_j\}_{j=1}^M$  are randomly chosen and fixed [4]. A common choice is the uniform distribution  $\mathbf{w}_j \sim \mathbb{U}([-R_m, R_m]^d)$  and  $b_j \sim \mathbb{U}([-R_m, R_m])$ , though different distributions can be used. The outer parameters  $\{a_j\}_{j=1}^M$  are free and the only ones subject to training. Consequently, the training process can be reduced to a convex optimization problem (least squares problem). The approximation capabilities of these two models have been extensively studied in the literature. Notable works include [1, 18, 16, 30], which investigate the approximation ability of neural networks; the approximation capabilities of the random feature model are studied in [22, 23].

## 2.2 PDE-solving Setup

We consider the following Poisson equation:

$$\begin{cases} -\Delta u = f & \text{in } \Omega, \\ u = 0 & \text{on } \partial\Omega. \end{cases} \quad (4)$$

Using a neural network structure, the training loss function of PINNs [24] is defined as:

$$L_{\text{PINN}}(\boldsymbol{\theta}) := L_{\text{F}}(\boldsymbol{\theta}) + \lambda L_{\text{B}}(\boldsymbol{\theta}) = \sum_{i=1}^N |\Delta\phi(\mathbf{x}_i; \boldsymbol{\theta}) - f(\mathbf{x})|^2 + \lambda \sum_{i=1}^{\hat{N}} |\phi(\mathbf{y}_i; \boldsymbol{\theta})|^2. \quad (5)$$

Here,  $L_{\text{F}}(\boldsymbol{\theta})$  represents the residual on PDE equations, while  $L_{\text{B}}(\boldsymbol{\theta})$  represents the boundary/initial condition. The variables  $\mathbf{x}_j \in \Omega$  and  $\mathbf{y}_j \in \partial\Omega$ , and  $\lambda$  is a constant used to balance the contributions from the domain and boundary terms.

## 3 AD v.s. FD Methods

When solving PDEs using neural networks, the derivatives appear in the loss function, Eq. 5, and are handled in two approaches: AD computes derivatives analytically via the chain rule [2, 24, 5], while FD approximates derivatives numerically based on local points [7, 19, 15, 20]. In this section, we compare AD and FD methods on the loss function of the PINN setup for both the random feature model and two-layer neural networks. Specifically, we investigate: (1) the truncated entropy of system matrix  $\mathbf{A}$  within the random feature method, and (2) the singular value distribution of the training kernel  $\mathbf{G}$  within the neural network. By analyzing these two models, we can evaluate how the differentiation methods affect the training process. For simplicity, we employ the one-dimensional Poisson equation  $u_{xx}(x) = f(x)$  with Dirichlet boundary conditions to illustrate our experimental and theoretical analysis. The exact solution of the equation is represented by  $u(x) = \sin(\pi x)$ , where  $x \in [-1, 1]$ .

### 3.1 AD v.s. FD for Random Feature Models

For simplicity, we focus on the differential equation residual loss (since the boundary condition does not involve derivatives) in Eq. 5, namely,

$$L_{\text{F}}(\mathbf{a}) := \sum_{i=1}^N |\phi_{xx}(x_i; \mathbf{a}) - f(x_i)|^2. \quad (6)$$

Here,  $x_i = i \cdot h$  and  $h = \frac{2}{N}$ . In this context, since we only need to train the parameters  $\{a_j\}_{j=1}^M$  in the random feature model, we use  $\phi(x; \mathbf{a})$  instead of  $\phi(x; \boldsymbol{\theta})$ .

To compute the second-order derivatives, the loss function with the AD method can be expressed as:

$$L_{\text{F}}^{\text{AD}}(\mathbf{a}) := \sum_{i=1}^N \left| \sum_{j=1}^M a_j w_j^2 (\sigma''(w_j \cdot x_i + b_j) - f(x_i)) \right|^2 = \|\mathbf{A}_{\text{AD}} \cdot \mathbf{a} - \mathbf{f}\|^2, \quad (7)$$

where  $\mathbf{A}_{AD} = (w_j^2(\sigma''(w_j \cdot x_i + b_j)))_{ij}$  and  $\mathbf{f} = [f(x_1), f(x_2), \dots, f(x_N)]^T$ . The solution can be computed as  $\mathbf{a} = \mathbf{A}_{AD}^\dagger \mathbf{f}$ , where  $\mathbf{A}_{AD}^\dagger = (\mathbf{A}_{AD}^T \mathbf{A}_{AD})^{-1} \mathbf{A}_{AD}^T$  is the pseudo-inverse of  $\mathbf{A}_{AD}$ .

The loss function with the FD method reads as:

$$L_F^{FD}(\mathbf{a}) = \sum_{i=1}^N \left| \sum_{j=1}^M a_j \frac{\sigma(w_j \cdot x_{i-1} + b_j) + \sigma(w_j \cdot x_{i+1} + b_j) - 2\sigma(w_j \cdot x_i + b_j)}{h^2} - f(x_i) \right|^2 \quad (8)$$

$$= \|\mathbf{A}_{FD} \cdot \mathbf{a} - \mathbf{f}\|^2,$$

where  $\mathbf{A}_{FD} = \mathbf{C}_2 \cdot \mathbf{A}_0$  as shown in Eq. 12 below. The solution can be computed as  $\mathbf{a} = \mathbf{A}_{FD}^\dagger \mathbf{f}$ , where  $\mathbf{A}_{FD}^\dagger = (\mathbf{A}_{FD}^T \mathbf{A}_{FD})^{-1} \mathbf{A}_{FD}^T$  is the pseudo-inverse of  $\mathbf{A}_{FD}$ .

In this section, we will analyze the training process of these two methods based on the singular values of  $\mathbf{A}_{AD}$  or  $\mathbf{A}_{FD}$ , i.e., the positive square root of eigenvalues of  $\mathbf{A}_{AD}^T \mathbf{A}_{AD}$  and  $\mathbf{A}_{FD}^T \mathbf{A}_{FD}$ . First of all, we want to mention that the large singular values are close for the two matrices since when  $h$  is small, the gap between the two matrices is small, i.e.,

$$\mathbf{A}_{AD} = \mathbf{A}_{FD} + h^2 \mathbf{E}, \quad (9)$$

where  $\mathbf{E}$  is the numerical differentiation errors matrix. Hence, the difference in eigenvalues between the two matrices is  $\mathcal{O}(h^2)$ , which will affect the small singular values a lot but not the large singular values. Mathematically, we can show that

**Proposition 1.** *Suppose  $\mathbf{E}^T \mathbf{A}_{FD} + \mathbf{A}_{FD}^T \mathbf{E} + h^2 \mathbf{E}^T \mathbf{E}$  is positive and the largest eigenvalue is  $\bar{\lambda}$ , we have that*

$$\lambda_{\max}(\mathbf{A}_{FD}^T \mathbf{A}_{FD}) \leq \lambda_{\max}(\mathbf{A}_{AD}^T \mathbf{A}_{AD}) \leq \lambda_{\max}(\mathbf{A}_{FD}^T \mathbf{A}_{FD}) + h^2 \bar{\lambda}. \quad (10)$$

For the small eigenvalues, based on the following Proposition 2, we know that the small eigenvalue, i.e., the eigenvalue in  $\mathcal{O}(h^2)$  level,  $\mathbf{A}_{AD}^T \mathbf{A}_{AD}$ , should be smaller than  $\mathbf{A}_{FD}^T \mathbf{A}_{FD}$ .

Denoting  $\mathbf{A}_0 = (\sigma(w_j \cdot x_i + b_j))_{ij}$  and  $\mathbf{A}_2 = (\sigma''(w_j \cdot x_i + b_j))_{ij}$ , we have that

$$\mathbf{A}_{AD} = \mathbf{A}_2 \cdot \mathbf{D}_2, \quad \mathbf{A}_{FD} = \mathbf{C}_2 \cdot \mathbf{A}_0 \quad (11)$$

where

$$\mathbf{C}_2 = \frac{1}{h^2} \begin{bmatrix} -2 & 1 & & & \\ 1 & -2 & 1 & & \\ & \ddots & \ddots & \ddots & \\ & & 1 & -2 & 1 \\ & & & 1 & -2 \end{bmatrix} \in \mathbb{R}^{N \times N}, \quad \mathbf{D}_2 = \begin{bmatrix} w_1^2 & & \\ & \ddots & \\ & & w_M^2 \end{bmatrix} \in \mathbb{R}^{M \times M}. \quad (12)$$

**Proposition 2.** *Suppose  $M = N$  and  $\mathbf{A}_{FD}, \mathbf{A}_{AD}$  is invertible, we have*

$$\lambda_{\min}(\mathbf{A}_{FD}) \geq \lambda_{\min}(\mathbf{A}_0) \lambda_{\min}(\mathbf{C}_2), \quad \lambda_{\min}(\mathbf{A}_2) \geq \lambda_{\min}(\mathbf{A}_{AD}) \lambda_{\min}(\mathbf{D}_2^{-1}). \quad (13)$$

The proof of Proposition 1 and Proposition 2 is given in the appendix.

For Proposition 2, if we omit the effect of the activation function, since for smooth functions like  $\sin(x)$  and  $\arctan(x)$ , the eigenvalues of the derivative matrix are in the same order of magnitude as the original matrix. In other words, we have  $\lambda_{\min}(\mathbf{A}_0) \geq C \lambda_{\min}(\mathbf{A}_2)$ , where  $C$  is a term of order  $\mathcal{O}(1)$ . Due to  $\lambda_{\min}(\mathbf{C}_2) = 4N^2 \cos^2 \frac{N\pi}{2N+1} \geq 1$  [32], and  $\lambda_{\min}(\mathbf{D}_2^{-1}) \geq 1$  if we randomly choose  $w_i \sim \mathbb{U}([-1, 1]^d)$ , we have

$$\lambda_{\min}(\mathbf{A}_{FD}) \geq C \lambda_{\min}(\mathbf{C}_2) \lambda_{\min}(\mathbf{D}_2^{-1}) \lambda_{\min}(\mathbf{A}_{AD}).$$

When  $C \geq \frac{1}{\lambda_{\min}(\mathbf{C}_2) \lambda_{\min}(\mathbf{D}_2^{-1})}$ , we have  $\lambda_{\min}(\mathbf{A}_{FD}) \geq \lambda_{\min}(\mathbf{A}_{AD})$ .

We conducted experiments using the random feature method, where we varied the activation functions and dimensions to solve the Poisson equation. Here we choose  $w_j$  and  $b_j$  from uniform distribution  $\mathbb{U}([-1, 1])$ . As depicted in Fig. 2, we observe that the large singular values of  $\mathbf{A}_{FD}$  and  $\mathbf{A}_{AD}$  are close, but the small eigenvalue of  $\mathbf{A}_{FD}$  is larger than  $\mathbf{A}_{AD}$  confirming the analysis presented earlier.

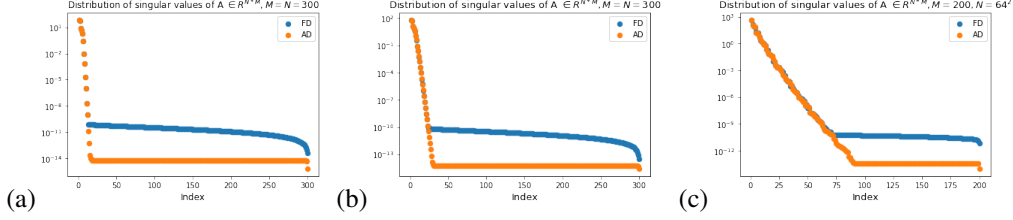


Figure 2: Distribution of singular values for  $\mathbf{A}_{\text{FD}}$  and  $\mathbf{A}_{\text{AD}}$  for solving Poisson equation using Random Feature Method with vary Dimensions  $d$ , Activation Functions  $\sigma(x)$ , Number of Sample Points  $N$  and Number of Neurons  $M$ . **(a)**:  $d = 1$ ,  $\sigma(x) = \sin(x)$ ,  $M = N = 100$ . **(b)**:  $d = 1$ ,  $\sigma(x) = \tanh(x)$ ,  $M = N = 300$ . **(c)**:  $d = 2$ ,  $\sigma(x) = \sin(x)$ ,  $M = 200$ ,  $N = 64 \times 64$ .

The distinction between the AD and FD methods in solving PDEs using random feature models can be elucidated by analyzing the differential characteristics of the singular values of  $\mathbf{A}_{\text{AD}}$  and  $\mathbf{A}_{\text{FD}}$ . Minimizing  $L_F^{\text{AD}}(\mathbf{a})$  and  $L_F^{\text{FD}}(\mathbf{a})$  can be reformulated as solving the linear systems  $\mathbf{A}_{\text{AD}}\mathbf{a} = \mathbf{f}$  and  $\mathbf{A}_{\text{FD}}\mathbf{a} = \mathbf{f}$ , respectively. To solve  $\mathbf{A}\mathbf{a} = \mathbf{f}$ , it is often necessary to compute the pseudo-inverse of matrix  $\mathbf{A}$ . However, if the non-zero singular values are too small, the computation error becomes large. To mitigate computation errors, it is common practice to do truncation based on singular values of matrix  $\mathbf{A}$ . In this study, we utilize the truncated SVD method to analyze the influence of eigenvalues on the training error. We denote the singular values of  $\mathbf{A}_{\text{AD}}$  as  $\{\sigma_i\}_{i=1}^M$  and those of  $\mathbf{A}_{\text{FD}}$  as  $\{\hat{\sigma}_i\}_{i=1}^M$ . The SVD decomposition of  $\mathbf{A}_{\text{AD}}$  and  $\mathbf{A}_{\text{FD}}$  can be expressed as follows:

$$\mathbf{A}_{\text{AD}} = \sum_{i=1}^P \sigma_i u_i v_i^T + \sum_{i=K+1}^M \sigma_i u_i v_i^T, \quad \mathbf{A}_{\text{FD}} = \sum_{i=1}^{\hat{P}} \hat{\sigma}_i \hat{u}_i \hat{v}_i^T + \sum_{i=\hat{K}+1}^M \hat{\sigma}_i \hat{u}_i \hat{v}_i^T, \quad (14)$$

where  $P$  and  $\hat{P}$  are the truncated positions. Then the truncated matrix can be expressed as  $\tilde{\mathbf{A}}_{\text{AD}} = \sum_{i=1}^P \sigma_i u_i v_i^T$ ,  $\tilde{\mathbf{A}}_{\text{FD}} = \sum_{i=1}^{\hat{P}} \hat{\sigma}_i \hat{u}_i \hat{v}_i^T$ . By direct calculation, the truncation error can be expressed as

$$\epsilon_{\text{AD}} := \|\mathbf{A}_{\text{AD}} - \tilde{\mathbf{A}}_{\text{AD}}\|^2 = \sum_{i=P+1}^M \sigma_i^2, \quad \epsilon_{\text{FD}} := \|\mathbf{A}_{\text{FD}} - \tilde{\mathbf{A}}_{\text{FD}}\|^2 = \sum_{i=\hat{P}+1}^M \hat{\sigma}_i^2.$$

Thus the training error can be formulated as

$$\|\mathbf{A}_{\text{AD}} \cdot \mathbf{a} - \mathbf{f}\|^2 \leq \|\tilde{\mathbf{A}}_{\text{AD}} \cdot \mathbf{a} - \mathbf{f}\|^2 + \epsilon_{\text{AD}}, \quad \|\mathbf{A}_{\text{FD}} \cdot \mathbf{a} - \mathbf{f}\|^2 \leq \|\tilde{\mathbf{A}}_{\text{FD}} \cdot \mathbf{a} - \mathbf{f}\|^2 + \epsilon_{\text{FD}}. \quad (15)$$

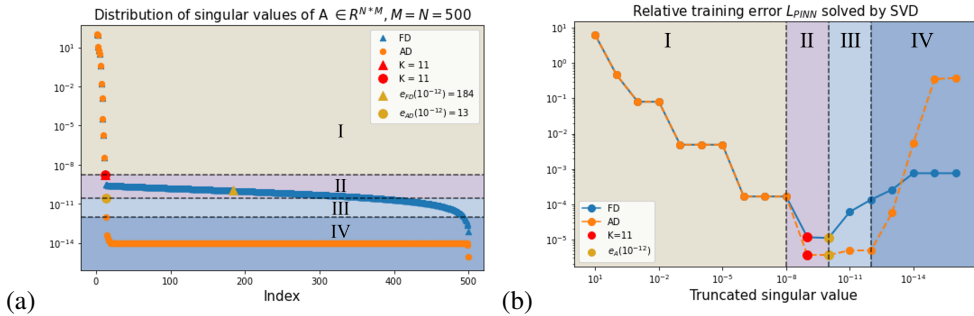


Figure 3: **(a)**: The distribution of singular values alongside their respective truncation positions. Yellow dots represent truncated positions based on  $e_A(10^{-12})$ , with *truncated entropy* values of  $H_{\mathbf{A}_{\text{FD}}}(10^{-12}) = 0.0056$  and  $H_{\mathbf{A}_{\text{AD}}}(10^{-12}) = 0.0866$ . **(b)**: Relative training error of  $L_{\text{PINN}}$ , denoted as  $\frac{\|\mathbf{A}\mathbf{a} - \mathbf{f}\|}{\|\mathbf{f}\|}$ , obtained using the truncated singular value decomposition (SVD) method. The horizontal axis represents the truncation position determined by the effective cut-off number.

The experiment results are shown in Fig. 3. We determine the truncated positions based on *effective cut-off number*, i.e.,  $P = e_{\mathbf{A}_{\text{AD}}}(a)$  and  $\hat{P} = e_{\mathbf{A}_{\text{FD}}}(a)$ . We can divide the truncated position

into four stages based on the relationship between training error and the truncated position. In **Stage I**, the truncated position  $P = \hat{P} < K$ , where  $K$  represents the last similar singular value shared by  $\mathbf{A}_{\text{AD}}$  and  $\mathbf{A}_{\text{FD}}$ , as indicated by the red dot in Fig. 3(a). The training errors for AD and FD are similar in this stage because the training error is dominated by  $\epsilon_{\text{AD}} \approx \sum_{i=P+1}^K \sigma_i^2 \approx \epsilon_{\text{FD}} \approx \sum_{i=P+1}^K \hat{\sigma}_i^2$ . In **Stage II**, the truncated position  $P \geq K$ . The red and yellow data points in the Fig. 3(b), the training error of AD is smaller than FD. The training error is dominated by  $\epsilon_{\text{AD}} \approx \sum_{i=P+1}^M \sigma_i^2 < \epsilon_{\text{FD}} \approx \sum_{i=P+1}^M \hat{\sigma}_i^2$ . In **Stage III** and **Stage IV**, we observe that increasing the truncation position  $P$  leads to an increase in training error. At this time, the training error is dominated by  $\|\tilde{\mathbf{A}}_{\text{AD}} \cdot \mathbf{a} - \mathbf{f}\|^2$  and  $\|\tilde{\mathbf{A}}_{\text{FD}} \cdot \mathbf{a} - \mathbf{f}\|^2$  caused by computation errors that arise when computing the pseudo-inverse of the truncated matrix. The yellow dot in the Fig. 3 represents  $P = e_{\mathbf{A}}(10^{-12})$ , which indicates the truncated position that can be computed without introducing significant computational errors when using the SVD method. If  $P > e_{\mathbf{A}}(10^{-12})$ , it would lead to substantial computational errors. Therefore, we can say that in the given scenario, the effective cut-off number is  $e_{\mathbf{A}}(10^{-12})$ . By calculating the corresponding truncated entropy we have  $H_{\mathbf{A}_{\text{AD}}}(10^{-12}) = 0.0866 > H_{\mathbf{A}_{\text{FD}}}(10^{-12}) = 0.0056$ . The truncated entropy of AD is larger than that of FD. i.e.,  $H_{\mathbf{A}_{\text{AD}}}(10^{-12}) > H_{\mathbf{A}_{\text{FD}}}(10^{-12})$ , and AD exhibits a smaller training error compared to FD.

The variation of training error with the truncated position in the Truncated SVD method can provide insights for training in the following neural network case.

### 3.2 AD vs. FD for two-layer Neural Networks

In contrast to random feature models, for neural networks, the parameters in the activation functions are free, and we cannot directly solve the optimization problem using methods like  $\mathbf{A}\mathbf{a} = \mathbf{f}$ , as this problem is non-convex. To tackle such optimization problems, there are various methods available, including gradient descent [26], stochastic gradient descent [33], Adam method [13], Gauss-Newton method [10], preconditioned methods [11], homotopy methods [28], and others. Each of these methods has its pros and cons, and the choice of method depends on the specific characteristics of the optimization problem and the desired properties of the solution. Here our analysis is based on the gradient descent method.

Due to the structure of neural networks, there are two kinds of parameters: one is outside the activation functions, i.e.,  $\{a_j\}_{j=1}^M$ , and the other is inside the activation function,  $\{w_j, b_j\}_{j=1}^M$  (Eq. 3). For parameters  $\{a_j\}_{j=1}^M$ , the gradient descent can be expressed as:

$$\frac{d\mathbf{a}}{dt} = -2\mathbf{A}_\kappa^\top (\Delta_\kappa \phi(\mathbf{x}; \boldsymbol{\theta}) - f(\mathbf{x})), \quad (16)$$

where  $\mathbf{A}_\kappa = \mathbf{A}_{\text{AD}}$  for AD method and  $\mathbf{A}_\kappa = \mathbf{A}_{\text{FD}}$  for FD method. For the parameter  $\{w_i, b_i\}_{i=1}^M$ , we only consider  $w_i$  since  $b_i$  can be merged into  $w_i$  by setting  $\mathbf{x} = (x, 1)$ . The gradient descent of AD methods can be expressed as:

$$\frac{d\mathbf{w}}{dt} = -2(\mathbf{X} \cdot \mathbf{A}_3 \cdot \mathbf{D}_3 \cdot \bar{\mathbf{A}} + 2\mathbf{A}_2 \cdot \mathbf{D}_1 \cdot \bar{\mathbf{A}})^\top \cdot (\Delta_\kappa \phi(\mathbf{x}; \boldsymbol{\theta}) - f(\mathbf{x})), \quad (17)$$

where  $\mathbf{A}_3 = (\sigma^{(3)}(w_j \cdot x_i + b_j))_{ij}$ ,  $\bar{\mathbf{A}} = \text{diag}(a_1, \dots, a_M)$  and  $\mathbf{X} = \text{diag}(x_1, \dots, x_N)$ . For gradient descent in FD method, it can be expressed as:

$$\frac{d\mathbf{w}}{dt} = -2(\mathbf{C}_2 \cdot \mathbf{X} \cdot \mathbf{A}_1 \cdot \bar{\mathbf{A}})^\top (\Delta_\kappa \phi(\mathbf{x}; \boldsymbol{\theta}) - f(\mathbf{x})). \quad (18)$$

For the loss function  $L_{\text{F}}(\boldsymbol{\theta}) := \sum_{i=1}^N |\Delta_\kappa \phi(x_i; \boldsymbol{\theta}) - f(x_i)|^2$ . The gradient descent dynamics can be expressed as:

$$\frac{dL_{\text{F}}(\boldsymbol{\theta})}{dt} = \nabla_{\mathbf{a}} L_{\text{F}}(\boldsymbol{\theta}) \frac{d\mathbf{a}}{dt} + \nabla_{\mathbf{w}} L_{\text{F}}(\boldsymbol{\theta}) \frac{d\mathbf{w}}{dt} = -2(\Delta_\kappa \phi(\mathbf{x}; \boldsymbol{\theta}) - f(\mathbf{x}))^\top \mathbf{G}_\kappa (\Delta_\kappa \phi(\mathbf{x}; \boldsymbol{\theta}) - f(\mathbf{x})),$$

where

$$\begin{aligned} \mathbf{G}_{\text{AD}} &= \mathbf{A}_{\text{AD}} \mathbf{A}_{\text{AD}}^\top + (\mathbf{X} \cdot \mathbf{A}_3 \cdot \mathbf{D}_3 \cdot \bar{\mathbf{A}} + 2\mathbf{A}_2 \cdot \mathbf{D}_1 \cdot \bar{\mathbf{A}})(\mathbf{X} \cdot \mathbf{A}_3 \cdot \mathbf{D}_3 \cdot \bar{\mathbf{A}} + 2\mathbf{A}_2 \cdot \mathbf{D}_1 \cdot \bar{\mathbf{A}})^\top, \\ \mathbf{G}_{\text{FD}} &= \mathbf{A}_{\text{FD}} \mathbf{A}_{\text{FD}}^\top + (\mathbf{C}_2 \cdot \mathbf{X} \cdot \mathbf{A}_1 \cdot \bar{\mathbf{A}})(\mathbf{C}_2 \cdot \mathbf{X} \cdot \mathbf{A}_1 \cdot \bar{\mathbf{A}})^\top. \end{aligned} \quad (19)$$

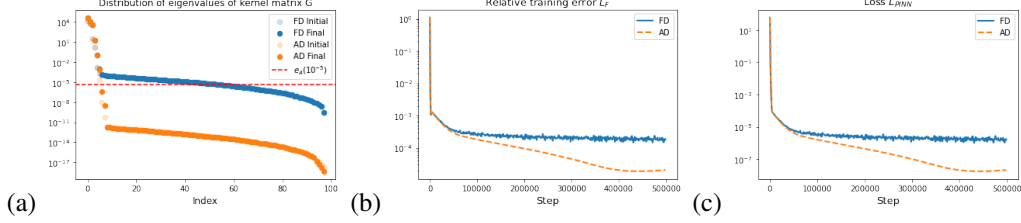


Figure 4: **(a)**: Distribution of eigenvalues of kernel matrix  $G$  with the red dashed line indicating the approximate convergence position  $e_{G_{\kappa}}(10^{-5})$  at the end of training. *Truncated entropy* values are  $H_{G_{FD}}(10^{-5}) = 0.0021$  and  $H_{G_{AD}}(10^{-5}) = 0.0250$ . **(b)**: Training curve of relative training error  $\frac{L_F}{\|f\|}$ . **(c)**: Training curve of the loss function  $L_{PINN}$ . (Similar performance observed for  $L_F$  and  $L_{PINN}$  due to the boundary conditions being treated as an identity operator.)

As depicted in Fig. 4(a), the eigenvalues of the kernel  $G$  in the gradient descent process for learning  $\theta$  exhibit similarities to those of system matrix  $A$  observed in the random feature model case. This is expected, given that the kernels  $G_{\kappa}$  tend to converge as  $h$  diminishes, reducing the magnitude of large eigenvalues (Proposition 1). Additionally,  $C_2$  in Eq. 12 serves to augment the small eigenvalues of the kernel in the finite difference (FD) method, surpassing those in the automatic differentiation (AD) methods (Proposition 2). A similar analysis applies to  $A_{\kappa}$ , and we refrain from elaborating further here. While the kernel undergoes changes during training, unlike in the random feature model, it's noteworthy that the eigenvalue relationship between the two methods remains consistent throughout training, as illustrated in Fig. 4(a). Based on Fig. 4(b), we can notice that in the beginning of the gradient descent, the performances of AD and FD methods are similar, which is due to the dominant role played by the large eigenvalues, that are similar. After several iteration steps in gradient descent, we notice that the speed of gradient descent in FD is slower than that of AD. This is due to the small eigenvalue direction beginning to play an important role in the training, and we can explain this theoretically as follows.

For the vector  $r_{AD} := \Delta_{AD}\phi(x; \theta) - f(x)$ , we perform the eigenvalue decomposition of  $A_{AD}^T A_{AD}$ , denoted as  $r_{AD} = \sum_{i=1}^M r_{i,AD}$  such that  $A_{AD} A_{AD}^T r_{i,AD} = \lambda_{i,AD} r_{i,AD}$  for  $\lambda_{1,AD} \geq \lambda_{2,AD} \geq \dots \geq \lambda_{M,AD}$ . Similarly, for finite difference method, we have  $r_{FD} := \Delta_{FD}\phi(x; \theta) - f(x) = \sum_{i=1}^M r_{i,FD}$  such that  $A_{FD} A_{FD}^T r_{i,FD} = \lambda_{i,FD} r_{i,FD}$  for  $\lambda_{1,FD} \geq \lambda_{2,FD} \geq \dots \geq \lambda_{M,FD}$ . Therefore, the gradient descent for two methods can be written as  $\frac{dL_{\kappa}(\theta)}{dt} = -2 \sum_{i=1}^M \lambda_{i,\kappa} r_{i,\kappa}^2$ . For eigenvalues smaller than  $a\sqrt{\lambda_1}$ , the training error can be considered negligible. This is similar to the truncated SVD in RFM, as shown in Fig. 3, the singular values  $\sigma < 10^{-12}\sigma_1$  can be truncated, given that the training error will not decrease post-truncation. Specifically,  $r_{i,FD} \approx 0$  for  $i > e_{G_{FD}}(a)$  and  $r_{i,AD} \approx 0$  for  $i > e_{G_{AD}}(a)$  throughout the entire learning process. Due to the similar performance of  $A_{\kappa}$  and  $G_{\kappa}$ , we assume the error in this part to be 0 in the gradient descent. This means we disregard these eigenvalues when determining loss convergence speed. Since large eigenvalues (for  $i > e_{G_{\kappa}}(b)$ ) converge fast, we consider the stage when the convergence speed is dominated by gradient descent of the kept small eigenvalues, i.e.,  $\frac{dL_{\kappa}(\theta)}{dt} = -2 \sum_{i=e_{G_{\kappa}}(b)}^{e_{G_{\kappa}}(a)} \lambda_{i,\kappa} r_{i,\kappa}^2$ . As stated in the following theorem:

**Theorem 1.** Suppose there exist a constant  $a, b, t_*$  such that  $r_{i,FD} = 0$  for  $i > e_{G_{FD}}(a)$ ,  $i < e_{G_{FD}}(b)$ , and  $r_{i,AD} = 0$  for  $i > e_{G_{AD}}(a)$ ,  $i < e_{G_{AD}}(b)$  for all  $t \geq t_*$ . For any  $T \geq t_*$ , we have that

$$\begin{aligned} & \exp \left( -2\zeta_{\kappa}(T) \cdot \max_{t \in [t_*, T]} \frac{\sum_{i=e_{G_{\kappa}}(b)}^{e_{G_{\kappa}}(a)} \lambda_{i,\kappa}}{e_{G_{\kappa}}(a) - e_{G_{\kappa}}(b)} (t - t_*) \right) \cdot L_{\kappa}(\theta)[t_*] \\ & \leq L_{\kappa}(\theta)[t] \leq \exp \left( -2\eta_{\kappa}(T) \cdot \min_{t \in [t_*, T]} \frac{\sum_{i=e_{G_{\kappa}}(b)}^{e_{G_{\kappa}}(a)} \lambda_{i,\kappa}}{e_{G_{\kappa}}(a) - e_{G_{\kappa}}(b)} (t - t_*) \right) \cdot L_{\kappa}(\theta)[t_*], \end{aligned} \quad (20)$$

for all  $t \in [t_*, T]$ , where  $\kappa = AD, FD$ , and

$$\eta_{\kappa}(T) = \min_{t \in [t_*, T]} \frac{\min\{r_{i,\kappa}^2\}_{i=e_{G_{\kappa}}(b)}^{e_{G_{\kappa}}(a)}}{\max\{r_{i,\kappa}^2\}_{i=e_{G_{\kappa}}(a)}} , \quad \zeta_{\kappa}(T) := \max_{t \in [t_*, T]} \frac{\max\{r_{i,\kappa}^2\}_{i=e_{G_{\kappa}}(b)}^{e_{G_{\kappa}}(a)}}{\min\{r_{i,\kappa}^2\}_{i=e_{G_{\kappa}}(a)}}$$

**Remark 1.** All the terms in Theorem 1 change with respect to the time  $t$  during the training. Suppose for the two methods,  $\eta_{AD}(T)$ ,  $\zeta_{AD}(T)$  and  $\eta_{FD}(T)$ ,  $\zeta_{FD}(T)$  are close, we can know that the speed of the AD method is faster than the FD methods due to when  $e_G(10^{-5}) > i > e_G(10^{-4})$  as shown in Fig. 4,

$$H_{G_{AD}}(a) \approx \frac{\sum_{i=e_{G_{AD}}(a)}^{e_{G_{AD}}(b)} \lambda_{i,AD}}{e_{G_{AD}}(a) - e_{G_{AD}}(b)} \gg \frac{\sum_{i=e_{G_{FD}}(a)}^{e_{G_{FD}}(b)} \lambda_{i,FD}}{e_{G_{FD}}(a) - e_{G_{FD}}(b)} \approx H_{G_{FD}}(a)$$

during the training process. This means that Truncated entropy can serve as an indicator of loss convergence speed.

## 4 Numerical results

In this section, we apply both the random feature models (RFM) and two-layer Neural Networks(NN) methods discussed in Section.3.1 and Section.3.2 to the Poisson equation in 2D and a fourth-order equation in 1D. This will demonstrate the effectiveness of AD compared to FD. In the case of the random feature model, the system precision is set to double, while for the neural network model, the system precision is set to float. Detailed experimental setups are provided in the appendix.

**Poisson Equation in 2D.** Consider the Poisson equation in 2D with the Dirichlet boundary condition over  $\Omega = [0, 1] \times [0, 1]$ , namely,  $-\Delta u(x, y) = f(x, y)$ ,  $(x, y) \in \Omega$ , and  $u(x, y) = 0$ ,  $(x, y) \in \partial\Omega$ . By choosing  $f(x) = \pi^2 \sin(\pi x) \sin(\pi y)$ , we have the exact solution is  $u(x, y) = \sin(\pi x) \sin(\pi y)$ .

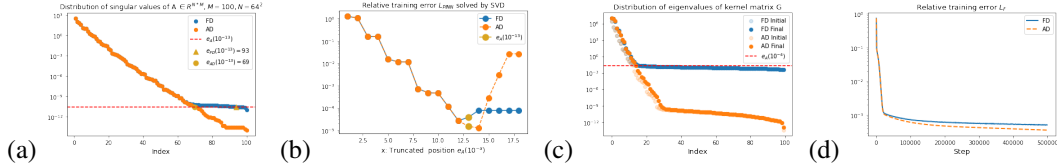


Figure 5: **Poisson Equation in 2D.** (a): Distribution of singular values of the random feature matrix  $A_k$  with the red dashed line indicating the effective cut-off number is  $e_{G_k}(10^{-13})$ . The *truncated entropy* values are  $H_{A_{FD}}(10^{-13}) = 0.0152$  and  $H_{A_{AD}}(10^{-13}) = 0.0200$ . (b): Relative training error of  $L_{PINN}$ , denoted as  $\frac{\|A_k a - f\|}{\|f\|}$ , obtained using the truncated SVD method. The horizontal axis represents the truncation determined by the effective cut-off number. (c): Distribution of eigenvalues of kernel matrix  $G$  with the red dashed line indicating the approximate convergence position  $e_{G_k}(10^{-4})$  at the end of training. The *truncated entropy* values are  $H_{G_{FD}}(10^{-4}) = 0.0771$  and  $H_{G_{AD}}(10^{-4}) = 0.0847$ . (d): Training curve of relative training error  $\frac{L_F}{\|f\|}$ .

In 2D Poisson equation, the detailed differences between  $L_F^{AD}$  and  $L_F^{FD}$  are described in the appendix. As shown in Fig. 5 it can be observed that the distribution of singular values of matrix  $A$  in the RFM and the distribution of eigenvalues of matrix  $G$  in the NN exhibit the same relationship between the AD and FD methods as described in the previous analysis. By comparing with the 1D scenario, it can be observed that the difference in truncated entropy between AD and FD is not significant, resulting in a similar training error. However, AD still outperforms FD.

**Biharmonic Equation.** We consider the fourth-order two-point boundary value problem  $\frac{d^4 u(x)}{dx^4} = \exp(x)$  with boundary conditions  $u(-1) = u(1) = 0$  and  $u'(-1) = u'(1) = 0$ . The exact solution is  $u(x) = c_0 + c_1 x + c_2 x^2 + c_3 x^3 + \exp(x)$  with  $c_0 = -\frac{5}{12}e^{-1} - \frac{1}{4}e$ ,  $c_1 = \frac{1}{2}e^{-1} - \frac{1}{2}e$ ,  $c_2 = \frac{1}{4}e^{-1} - \frac{1}{4}e$ ,  $c_3 = -\frac{1}{3}e^{-1}$ .

Due to the high order derivatives, the difference in the singular values distribution of  $A$  and eigenvalue distribution of  $G$  between AD and FD becomes more pronounced, as shown in Fig. 6. This leads to a larger difference in truncated entropy and thus AD significantly outperforms FD. We summarized the detailed differences between  $L_F^{AD}$  and  $L_F^{FD}$  in the appendix.

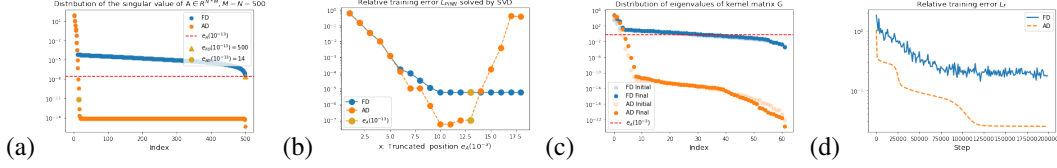


Figure 6: **Biharmonic Equation.** (a): Distribution of singular values of the random feature  $A_k$  with the red dashed line indicating the effective cut-off number is  $e_{G_k}(10^{-13})$ . The *truncated entropy* values are  $H_{A_{FD}}(10^{-13}) = 0.0023$  and  $H_{A_{AD}}(10^{-13}) = 0.0841$ . (b): Relative training error of  $L_{PINN}$ , denoted as  $\frac{\|A_k \alpha - f\|}{\|f\|}$ , obtained using the truncated SVD method. The horizontal axis represents the truncation position determined by the effective cut-off number. (c): Distribution of eigenvalues of kernel matrix  $G$  with the red dashed line indicating the approximate convergence position  $e_{G_k}(10^{-2})$  at the end of training. The *truncated entropy* values are  $H_{G_{FD}}(10^{-2}) = 0.0332$  and  $H_{G_{AD}}(10^{-2}) = 0.1872$ . (d): Training curve of relative training error  $\frac{L_F}{\|f\|}$ .

## 5 Conclusions

In this paper, we study the performance of AD and FD methods in training neural network structures to solve PDEs, including random feature models and two-layer neural networks. Our analysis of eigenvalues shows that the small eigenvalues of AD are smaller than those of FD methods, leading to superior performance in both SVD for random feature models and gradient descent for neural networks. To describe the influence of eigenvalues on training error, we introduce the concepts of *Effective cut-off number* and *Truncated entropy*, observing that larger *Truncated entropy* corresponds to smaller training error. Based on our findings, under the same settings, the truncated entropy of AD is larger than that of FD, predicting that AD outperforms FD methods in the training process. This analysis can extend to general neural network training scenarios, with *Truncated entropy* as an indicator of loss convergence speed. While this study focuses on two-layer networks, future research could explore deeper networks, different architectures like CNNs and Transformers, and other optimization algorithms such as pre-conditioners to accelerate convergence.

## Acknowledgments and Disclosure of Funding

Y.Y. and W.H. was supported by National Institute of General Medical Sciences through grant 1R35GM146894. The work of Y.X. was supported by the Project of Hetao Shenzhen-HKUST Innovation Cooperation Zone HZQB-KCZYB-2020083.

## References

- [1] A. Barron. Universal approximation bounds for superpositions of a sigmoidal function. *IEEE Transactions on Information theory*, 39(3):930–945, 1993.
- [2] A. Baydin, B. Pearlmutter, A. Radul, and J. Siskind. Automatic differentiation in machine learning: a survey. *Journal of machine learning research*, 18(153):1–43, 2018.
- [3] S. Cao. Choose a transformer: Fourier or galerkin. *Advances in neural information processing systems*, 34:24924–24940, 2021.
- [4] J. Chen, X. Chi, Z. Yang, et al. Bridging traditional and machine learning-based algorithms for solving pdes: the random feature method. *J Mach Learn*, 1:268–98, 2022.
- [5] Pao-Hsiung Chiu, Jian Cheng Wong, Chinchun Ooi, My Ha Dao, and Yew-Soon Ong. Can-pinn: A fast physics-informed neural network based on coupled-automatic-numerical differentiation method. *Computer Methods in Applied Mechanics and Engineering*, 395:114909, 2022.
- [6] D. Frenkel and B. Smit. *Understanding molecular simulation: from algorithms to applications*. Elsevier, 2023.
- [7] C. Grossmann. *Numerical treatment of partial differential equations*. Springer, 2007.

- [8] R. Guo, S. Cao, and L. Chen. Transformer meets boundary value inverse problems. In *The Eleventh International Conference on Learning Representations*, 2022.
- [9] J. Han, A. Jentzen, and W. E. Solving high-dimensional partial differential equations using deep learning. *Proceedings of the National Academy of Sciences*, 115(34):8505–8510, 2018.
- [10] W. Hao, Q. Hong, X. Jin, and Y. Wang. Gauss newton method for solving variational problems of pdes with neural network discretizations. *arXiv preprint arXiv:2306.08727*, 2023.
- [11] H. He, Z. Tang, S. Zhao, Y. Saad, and Y. Xi. nltgcr: A class of nonlinear acceleration procedures based on conjugate residuals. *SIAM Journal on Matrix Analysis and Applications*, 45(1):712–743, 2024.
- [12] Q. Hong, J. Siegel, and J. Xu. A priori analysis of stable neural network solutions to numerical pdes. *arXiv preprint arXiv:2104.02903*, 2021.
- [13] D. Kingma and J. Ba. Adam: A method for stochastic optimization. *arXiv preprint arXiv:1412.6980*, 2014.
- [14] Y. Lan, Z. Li, J. Sun, and Y. Xiang. Dosnet as a non-black-box pde solver: When deep learning meets operator splitting. *Journal of Computational Physics*, 491:112343, 2023.
- [15] Kart Leong Lim, Rahul Dutta, and Mihai Rotaru. Physics informed neural network using finite difference method. In *2022 IEEE International Conference on Systems, Man, and Cybernetics (SMC)*, pages 1828–1833. IEEE, 2022.
- [16] J. Lu, Y. Lu, and M. Wang. A priori generalization analysis of the Deep Ritz method for solving high dimensional elliptic partial differential equations. In *Conference on Learning Theory*, pages 3196–3241. PMLR, 2021.
- [17] J. Lu, Z. Shen, H. Yang, and S. Zhang. Deep network approximation for smooth functions. *SIAM Journal on Mathematical Analysis*, 53(5):5465–5506, 2021.
- [18] H. Mhaskar. Neural networks for optimal approximation of smooth and analytic functions. *Neural computation*, 8(1):164–177, 1996.
- [19] Ravi G. Patel, Indu Manickam, Nathaniel A. Trask, Mitchell A. Wood, Myoungkyu Lee, Ignacio Tomas, and Eric C. Cyr. Thermodynamically consistent physics-informed neural networks for hyperbolic systems. *Journal of Computational Physics*, 449:110754, 2022.
- [20] Timothy Praditia, Matthias Karlbauer, Sebastian Otte, Sergey Oladyshkin, Martin V Butz, and Wolfgang Nowak. Finite volume neural network: Modeling subsurface contaminant transport. *arXiv preprint arXiv:2104.06010*, 2021.
- [21] De R. and S. Mishra. Error analysis for physics-informed neural networks (pinns) approximating kolmogorov pdes. *Advances in Computational Mathematics*, 48(6):79, 2022.
- [22] A. Rahimi and B. Recht. Uniform approximation of functions with random bases. In *2008 46th annual allerton conference on communication, control, and computing*, pages 555–561. IEEE, 2008.
- [23] A. Rahimi and B. Recht. Weighted sums of random kitchen sinks: Replacing minimization with randomization in learning. *Advances in neural information processing systems*, 21, 2008.
- [24] M. Raissi, P. Perdikaris, and G. Karniadakis. Physics-informed neural networks: A deep learning framework for solving forward and inverse problems involving nonlinear partial differential equations. *Journal of Computational Physics*, 378:686–707, 2019.
- [25] O. Roy and M. Vetterli. The effective rank: A measure of effective dimensionality. In *2007 15th European signal processing conference*, pages 606–610. IEEE, 2007.
- [26] S. Ruder. An overview of gradient descent optimization algorithms. *arXiv preprint arXiv:1609.04747*, 2016.

- [27] J. Siegel, Q. Hong, X. Jin, W. Hao, and J. Xu. Greedy training algorithms for neural networks and applications to pdes. *Journal of Computational Physics*, 484:112084, 2023.
- [28] Y. Yang, Q. Chen, and W. Hao. Homotopy relaxation training algorithms for infinite-width two-layer relu neural networks. *arXiv preprint arXiv:2309.15244*, 2023.
- [29] Y. Yang and J. He. Deeper or wider: A perspective from optimal generalization error with sobolev loss. *International Conference on Machine Learning*, 2024.
- [30] Y. Yang, H. Yang, and Y. Xiang. Nearly optimal vc-dimension and pseudo-dimension bounds for deep neural network derivatives. *Advances in Neural Information Processing Systems*, 36, 2024.
- [31] B. Yu et al. The deep ritz method: a deep learning-based numerical algorithm for solving variational problems. *Communications in Mathematics and Statistics*, 6(1):1–12, 2018.
- [32] W. Yueh. Eigenvalues of several tridiagonal matrices. *Applied Mathematics E-Notes [electronic only]*, 5:66–74, 2005.
- [33] M. Zinkevich, M. Weimer, L. Li, and A. Smola. Parallelized stochastic gradient descent. *Advances in neural information processing systems*, 23, 2010.

## A Proof

### A.1 Proofs of Proposition 1 and 2

*Proof of Proposition 1.* First of all, we prove

$$\lambda_{\max}(\mathbf{A}_{AD}^T \mathbf{A}_{AD}) \leq \lambda_{\max}(\mathbf{A}_{FD}^T \mathbf{A}_{FD}) + h^2 \bar{\lambda}.$$

Since

$$\mathbf{A}_{AD}^T \mathbf{A}_{AD} = \mathbf{A}_{FD}^T \mathbf{A}_{FD} + h^2(\mathbf{E}^T \mathbf{A}_{FD} + \mathbf{A}_{FD}^T \mathbf{E}) + h^6 \mathbf{E}^T \mathbf{E}, \quad (\text{A.1.1})$$

we have

$$[\lambda_{\max}(\mathbf{A}_{FD}^T \mathbf{A}_{FD}) + h^2 \bar{\lambda}] \cdot \mathbf{I} - \mathbf{A}_{AD}^T \mathbf{A}_{AD} \quad (\text{A.1.2})$$

is a positive matrix. For any eigenvalue of  $\mathbf{A}_{AD}^T \mathbf{A}_{AD}$ ,  $\lambda$ ,  $\mathbf{A}_{AD}^T \mathbf{A}_{AD} \mathbf{v} = \lambda \mathbf{v}$ , we have

$$[\lambda_{\max}(\mathbf{A}_{FD}^T \mathbf{A}_{FD}) + h^2 \bar{\lambda}] \cdot \mathbf{I} \cdot \mathbf{v} - \mathbf{A}_{AD}^T \mathbf{A}_{AD} \mathbf{v} = (\lambda_{\max}(\mathbf{A}_{FD}^T \mathbf{A}_{FD}) + h^2 \bar{\lambda} - \lambda) \mathbf{v}. \quad (\text{A.1.3})$$

Hence

$$\lambda_{\max}(\mathbf{A}_{FD}^T \mathbf{A}_{FD}) + h^2 \bar{\lambda} - \lambda \geq 0,$$

due to the arbitrary choice of  $\lambda$ , we obtain

$$\lambda_{\max}(\mathbf{A}_{AD}^T \mathbf{A}_{AD}) \leq \lambda_{\max}(\mathbf{A}_{FD}^T \mathbf{A}_{FD}) + h^2 \bar{\lambda}.$$

Now we prove the next part, we have

$$\lambda_{\max}(\mathbf{A}_{AD}^T \mathbf{A}_{AD}) \cdot \mathbf{I} - \mathbf{A}_{FD}^T \mathbf{A}_{FD} \quad (\text{A.1.4})$$

is a positive matrix. For any eigenvalue of  $\mathbf{A}_{FD}^T \mathbf{A}_{FD}$ ,  $\lambda$ ,  $\mathbf{A}_{FD}^T \mathbf{A}_{FD} \mathbf{v} = \lambda \mathbf{v}$ , we have

$$[\lambda_{\max}(\mathbf{A}_{AD}^T \mathbf{A}_{AD}) \cdot \mathbf{I} - \mathbf{A}_{FD}^T \mathbf{A}_{FD}] \mathbf{v} = (\lambda_{\max}(\mathbf{A}_{AD}^T \mathbf{A}_{AD}) - \lambda) \mathbf{v}. \quad (\text{A.1.5})$$

Hence

$$\lambda_{\max}(\mathbf{A}_{FD}^T \mathbf{A}_{FD}) - \lambda \geq 0,$$

due to the arbitrary choice of  $\lambda$ , we obtain

$$\lambda_{\max}(\mathbf{A}_{FD}^T \mathbf{A}_{FD}) \leq \lambda_{\max}(\mathbf{A}_{AD}^T \mathbf{A}_{AD}).$$

□

*Proof of Proposition 2.* First of all, we know that for the symmetric positive matrices  $\mathbf{A}$  and  $\mathbf{B}$ ,  $\lambda_{\max}$  is a kind of sub-multiplicative norm, i.e.,

$$\lambda_{\max}(\mathbf{AB}) \leq \lambda_{\max}(\mathbf{A})\lambda_{\max}(\mathbf{B}).$$

By taking the inverse, we have

$$\lambda_{\min}(\mathbf{AB}) \geq \lambda_{\min}(\mathbf{A})\lambda_{\min}(\mathbf{B}).$$

Therefore, we have

$$\begin{aligned} \lambda_{\min}(\mathbf{A}_{\text{FD}}^{\top} \mathbf{A}_{\text{FD}}) &= \lambda_{\min}(\mathbf{A}_0^{\top} \mathbf{C}^{\top} \mathbf{C}_2 \mathbf{A}_0) = \lambda_{\min}(\mathbf{C}_2 \mathbf{A}_0 \mathbf{A}_0^{\top} \mathbf{C}^{\top}) \\ &\leq \lambda_{\min}(\mathbf{A}_0 \mathbf{A}_0^{\top}) \lambda_{\min}^2(\mathbf{C}_2). \end{aligned} \quad (\text{A.1.6})$$

Therefore, we have

$$\lambda_{\min}(\mathbf{A}_{\text{FD}}) \geq \lambda_{\min}(\mathbf{A}_0) \lambda_{\min}(\mathbf{C}_2).$$

The other inequality is proved in the same way.  $\square$

## A.2 Proof of Theorem 1

*Proof of Theorem 1.* Due to  $\frac{dL_{\kappa}(\boldsymbol{\theta})}{dt} = -2 \sum_{i=1}^M \lambda_{i,\kappa} \mathbf{r}_{i,\kappa}^2$  and  $\mathbf{r}_{i,\kappa} = 0$  for  $i > e_{\mathbf{G}_{\kappa}}(a)$ ,  $i < e_{\mathbf{G}_{\kappa}}(b)$ , we have that

$$\begin{aligned} \frac{dL_{\kappa}(\boldsymbol{\theta})}{dt} &= -2 \sum_{i=e_{\mathbf{G}_{\kappa}}(b)}^{e_{\mathbf{G}_{\kappa}}(a)} \lambda_{i,\kappa} \mathbf{r}_{i,\kappa}^2 \\ &= \frac{-2 \sum_{i=e_{\mathbf{G}_{\kappa}}(b)}^{e_{\mathbf{G}_{\kappa}}(a)} \lambda_{i,\kappa} \mathbf{r}_{i,\kappa}^2}{\sum_{i=e_{\mathbf{G}_{\kappa}}(b)}^{e_{\mathbf{G}_{\kappa}}(a)} \mathbf{r}_{i,\kappa}^2} L_{\kappa}(\boldsymbol{\theta}) \\ &\leq -2 \frac{\min\{\mathbf{r}_{i,\kappa}^2\}_{i=e_{\mathbf{G}_{\kappa}}(b)}^{e_{\mathbf{G}_{\kappa}}(a)}}{\max\{\mathbf{r}_{i,\kappa}^2\}_{i=e_{\mathbf{G}_{\kappa}}(b)}^{e_{\mathbf{G}_{\kappa}}(a)}} \cdot \frac{\sum_{i=e_{\mathbf{G}_{\kappa}}(b)}^{e_{\mathbf{G}_{\kappa}}(a)} \lambda_{i,\kappa}}{e_{\mathbf{G}_{\kappa}}(a) - e_{\mathbf{G}_{\kappa}}(b)} L_{\kappa}(\boldsymbol{\theta}) \\ &\leq -2\eta_{\kappa}(T) \cdot \min_{t \in [t_*, T]} \frac{\sum_{i=e_{\mathbf{G}_{\kappa}}(b)}^{e_{\mathbf{G}_{\kappa}}(a)} \lambda_{i,\kappa}}{e_{\mathbf{G}_{\kappa}}(a) - e_{\mathbf{G}_{\kappa}}(b)} \cdot L_{\kappa}(\boldsymbol{\theta}). \end{aligned} \quad (\text{A.2.1})$$

Therefore, we have that

$$L_{\kappa}(\boldsymbol{\theta})[t] \leq \exp \left( -2\eta_{\kappa}(T) \cdot \min_{t \in [0, T]} \frac{\sum_{i=e_{\mathbf{G}_{\kappa}}(b)}^{e_{\mathbf{G}_{\kappa}}(a)} \lambda_{i,\kappa}}{e_{\mathbf{G}_{\kappa}}(a) - e_{\mathbf{G}_{\kappa}}(b)} (t - t_*) \right) \cdot L_{\kappa}(\boldsymbol{\theta})[t_*] \quad (\text{A.2.2})$$

for all  $t \in [t_*, T]$ . The proof for the other direction follows the same steps.  $\square$

## B Experimental Details

In this section, we include more details about the experiments shown in the main text. We describe the experimental details based on different equations.

### B.1 Training setting

In the case of the random feature model, the system precision is set to double, while for the neural network model, the system precision is set to float. We train neural networks using the SGD optimizer with full batch training. We perform a learning rate sweep ranging from 1e-3 to 1e-4. All random feature models are structured as 2-layer fully connected NN, a  $\sin(x)$  activation function, and with  $\mathbf{w}_j \sim \mathbb{U}([-1, 1]^d)$  and  $b_j \sim \mathbb{U}([-1, 1])$ . All neural networks are 2-layer fully connected NN, a  $\sin(x)$  activation function, and uniformly sample collocation points  $x$  on the domain. All experiments are run on a single NVIDIA 3070Ti GPU.

### B.2 Poisson Equation in 1D

#### Equation

$$\begin{cases} u_{xx}(x) = f(x), & x \in [-1, 1], \\ u(-1) = u(1) = 0. \end{cases} \quad (\text{B.2.1})$$

By choosing  $f(x) = -\pi^2 \sin(\pi x)$ , we have the exact solution is  $u(x) = \sin(\pi x)$ .

**Random feature models.** We include extra distribution of singular values of  $A_{AD}$  and  $A_{FD}$  for different  $M = N$  as shown in Fig. 1 in the main context. The activation function is  $\sin(x)$ .

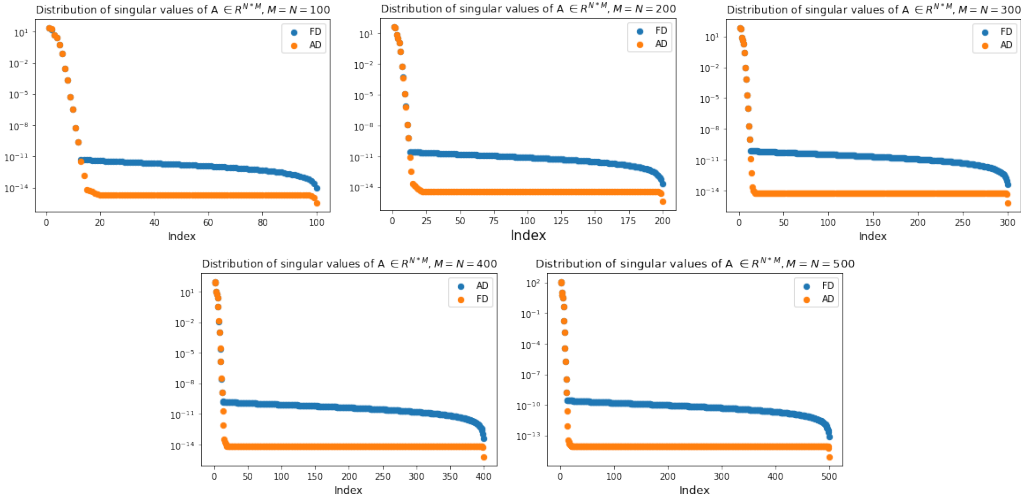


Figure B.2.1: Distribution of singular values of  $A_{AD}$  and  $A_{FD}$  for different settings of  $M = N$ .

**Neural Network.** As shown in Fig. 4 in the main context. Here, we use 2-layer fully connected NN with 100 neurons per layer, a  $\sin(x)$  activation function, and uniformly 100 sample collocation points. The loss function for AD and FD are defined as followed:

$$L_{\text{PINN}}^{\text{AD}}(\boldsymbol{\theta}) := L_{\text{F}}^{\text{AD}}(\boldsymbol{\theta}) + \lambda L_{\text{B}}(\boldsymbol{\theta}) = \frac{1}{N} \sum_{i=1}^N |\Delta \phi(\mathbf{x}_i; \boldsymbol{\theta}) - f(\mathbf{x})|^2 + \lambda \frac{1}{\hat{N}} \sum_{i=1}^{\hat{N}} |\phi(\mathbf{y}_i; \boldsymbol{\theta})|^2, \quad (\text{B.2.2})$$

$$\begin{aligned} L_{\text{PINN}}^{\text{FD}}(\boldsymbol{\theta}) &:= L_{\text{F}}^{\text{FD}}(\boldsymbol{\theta}) + \lambda L_{\text{B}}(\boldsymbol{\theta}) \\ &= \frac{1}{N} \sum_{i=1}^N \left| \frac{\phi(x_{i-1}; \boldsymbol{\theta}) + \phi(x_{i+1}; \boldsymbol{\theta}) - 2\phi(x_i; \boldsymbol{\theta})}{h^2} - f(x_i) \right|^2 + \lambda \frac{1}{\hat{N}} \sum_{i=1}^{\hat{N}} |\phi(\mathbf{y}_i; \boldsymbol{\theta})|^2, \end{aligned} \quad (\text{B.2.3})$$

where  $\lambda = 1$  and  $h = \frac{2}{100}$ .

### B.3 Poisson Equation in 2D.

#### Equation

$$\begin{cases} \Delta u(x, y) = f(x, y), & (x, y) \in \Omega, \\ u(x, y) = 0, & (x, y) \in \partial\Omega. \end{cases} \quad (\text{B.3.1})$$

By choosing  $f(x) = -\pi^2 \sin(\pi x) \sin(\pi y)$ , we have the exact solution is  $u(x, y) = \sin(\pi x) \sin(\pi y) \in [0, 1] \times [0, 1]$ .

**Random feature models.** In this case the  $M = 100$ ,  $N = 64 \times 64$   $\mathbf{A}_{\text{FD}} = \mathbf{C} \cdot \mathbf{A}_0$ .

$$\mathbf{C} = \frac{1}{h^2} \begin{bmatrix} D & -I & 0 & 0 & 0 & \cdots & 0 \\ -I & D & -I & 0 & 0 & \cdots & 0 \\ 0 & -I & D & -I & 0 & \cdots & 0 \\ \vdots & \ddots & \ddots & \ddots & \ddots & \ddots & \vdots \\ 0 & \cdots & 0 & -I & D & -I & 0 \\ 0 & \cdots & \cdots & 0 & -I & D & -I \\ 0 & \cdots & \cdots & \cdots & 0 & -I & D \end{bmatrix}$$

$I$  is the  $64 \times 64$  identity matrix, and  $D$ , also  $64 \times 64$ , is given by:

$$D = \begin{bmatrix} 4 & -1 & 0 & 0 & 0 & \cdots & 0 \\ -1 & 4 & -1 & 0 & 0 & \cdots & 0 \\ 0 & -1 & 4 & -1 & 0 & \cdots & 0 \\ \vdots & \ddots & \ddots & \ddots & \ddots & \ddots & \vdots \\ 0 & \cdots & 0 & -1 & 4 & -1 & 0 \\ 0 & \cdots & \cdots & 0 & -1 & 4 & -1 \\ 0 & \cdots & \cdots & \cdots & 0 & -1 & 4 \end{bmatrix}.$$

**Neural Network.** As shown in Fig. 5 in the main context. Here, we use 2-layer fully connected NN with 100 neurons per layer, a  $\sin(x)$  activation function, and uniformly  $N = 64 \times 64$  sample collocation points. The loss function for AD and FD are defined as followed:

$$L_{\text{PINN}}^{\text{AD}}(\boldsymbol{\theta}) := L_{\text{F}}^{\text{AD}}(\boldsymbol{\theta}) + \lambda L_{\text{B}}(\boldsymbol{\theta}) = \frac{1}{N} \sum_{i=1}^N |\Delta \phi_{xx}(x_i; \boldsymbol{\theta}) - f(x)|^2 + \lambda \frac{1}{\hat{N}} \sum_{i=1}^{\hat{N}} |\phi(\mathbf{y}_i; \boldsymbol{\theta})|^2, \quad (\text{B.3.2})$$

$$\begin{aligned} L_{\text{PINN}}^{\text{FD}}(\boldsymbol{\theta}) &:= L_{\text{F}}^{\text{FD}}(\boldsymbol{\theta}) + \lambda L_{\text{B}}(\boldsymbol{\theta}) \\ &= \frac{1}{N} \sum_{i=1}^N \left| \frac{\phi_{i+1,j} + \phi_{i-1,j} + \phi_{i,j-1} + \phi_{i,j+1} - e\phi_{i,j}}{h^2} - f(x_i) \right|^2 + \lambda \frac{1}{\hat{N}} \sum_{i=1}^{\hat{N}} |\phi(\mathbf{y}_i; \boldsymbol{\theta})|^2, \end{aligned} \quad (\text{B.3.3})$$

where  $\lambda = 1$  and  $h = \frac{1}{64}$  and  $\phi_{i,j} := \phi((x_i, y_j); \boldsymbol{\theta})$ .

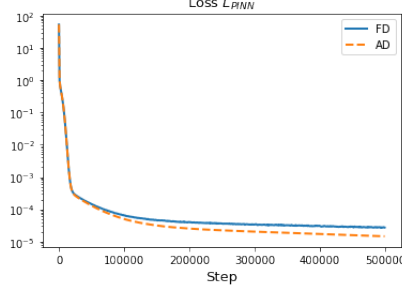


Figure B.3.1: Training curve of the loss function  $L_{PINN}$ .

#### B.4 Biharmonic Equation.

##### Equation

$$\frac{d^4 u(x)}{d^4 x} = \exp(x), \quad (\text{B.4.1})$$

with boundary conditions  $u(-1) = u(1) = 0$  and  $u'(-1) = u'(1) = 0$ . The exact solution is  $u(x) = c_0 + c_1 x + c_2 x^2 + c_3 x^3 + \exp(x)$  with  $c_1 = -\frac{5}{12}e^{-1} - \frac{1}{4}e$ ,  $c_2 = \frac{1}{2}e^{-1} - \frac{1}{2}e$ ,  $c_3 = \frac{1}{4}e^{-1} - \frac{1}{4}e$ ,  $c_0 = -\frac{1}{3}e^{-1}$ .

**Random feature models.** In this case the  $M = N = 500$   $\mathbf{A}_{FD} = \mathbf{C} \cdot \mathbf{A}_0$

$$\mathbf{C} = \frac{1}{h^4} \begin{bmatrix} -4 & 6 & -4 & 0 & 0 & \cdots & 0 \\ 1 & -4 & 6 & -4 & 1 & \cdots & 0 \\ 0 & 1 & -4 & 6 & -4 & \cdots & 0 \\ \vdots & \ddots & \ddots & \ddots & \ddots & \ddots & \vdots \\ 0 & \cdots & 4 & -6 & 4 & 1 & 0 \\ 0 & \cdots & \cdots & 4 & -6 & 4 & 1 \\ 0 & \cdots & \cdots & \cdots & 4 & -6 & 4 \end{bmatrix}$$

**Neural Network.** As shown in Fig. 5 in the main context. Here, we use 2-layer fully connected NN with 100 neurons per layer, a  $\sin(x)$  activation function, and uniformly  $\hat{N} = 64 \times 64$  sample collocation points. The loss function for AD and FD are defined as followed:

$$L_{PINN}^{AD}(\boldsymbol{\theta}) := L_F^{AD}(\boldsymbol{\theta}) + \lambda L_B(\boldsymbol{\theta}) = \frac{1}{N} \sum_{i=1}^N |\phi_{xxxx}(x_i; \boldsymbol{\theta}) - f(x)|^2 + \lambda \frac{1}{\hat{N}} \left( \sum_{i=1}^{\hat{N}} |\phi(y_i; \boldsymbol{\theta})|^2 + \sum_{i=1}^{\hat{N}} |\phi_x(y_i; \boldsymbol{\theta})|^2 \right), \quad (\text{B.4.2})$$

$$\begin{aligned} L_{PINN}^{FD}(\boldsymbol{\theta}) &:= L_F^{FD}(\boldsymbol{\theta}) + \lambda L_B(\boldsymbol{\theta}) \\ &= \frac{1}{N} \sum_{i=1}^N \left| \frac{\phi_{i-2} - 4\phi_{i-1} + 6\phi_i - 4\phi_{i+1} + \phi_{i+2}}{h^4} - f(x_i) \right|^2 + \lambda \frac{1}{\hat{N}} \left( \sum_{i=1}^{\hat{N}} |\phi(y_i; \boldsymbol{\theta})|^2 + \sum_{i=1}^{\hat{N}} |\phi_x(y_i; \boldsymbol{\theta})|^2 \right) \end{aligned} \quad (\text{B.4.3})$$

where  $\lambda = 100$  and  $h = \frac{1}{64}$  and  $\phi_i := \phi(x_i; \boldsymbol{\theta})$ .

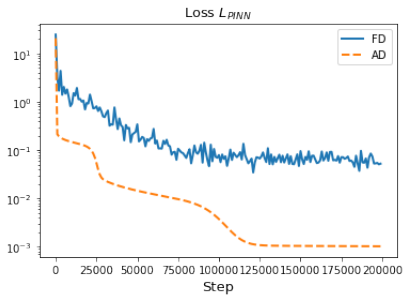


Figure B.4.1: Training curve of the loss function  $L_{PINN}$ .